Hindawi
Advances in Materials Science and Engineering
Volume 2019, Article ID 5253946, 11 pages
https://doi.org/10.1155/2019/5253946

Research Article

Development and Performance Test including Mechanical and Thermal of New Tenon Composite Block Masonry Walls

Hui Su,[1] **Dongyue Wu**,[2] **Mengying Shen**,[3] **Wei Chen**,[2] **and Shilin Wang**[2]

[1]*School of Architectural Engineering, Jinling Institute of Technology, Nanjing, China*
[2]*School of Civil Engineering and Architecture, Jiangsu University of Science and Technology, Zhenjiang, China*
[3]*Zhenjiang Archives, Zhenjiang, Jiangsu, China*

Correspondence should be addressed to Dongyue Wu; dywu@just.edu.cn

Received 31 May 2019; Revised 19 August 2019; Accepted 24 August 2019; Published 22 September 2019

Academic Editor: Giorgio Pia

To improve the thermal performance of external masonry walls, a new tenon composite block is proposed as the external maintenance component which contains the internal hollow concrete block part, the external block part, and the extruded polystyrene layer fixed by tenons. The production process and concrete material mixing ratio were optimized for the new tenon composite block to promote its application. The mechanical strength and thermal properties of the optimized tenon composite blocks were tested with experiments and numerical simulation in this study. The testing and simulation results indicated that after utilizing the two optimized concrete mixing ratios, the tenon composite block strength matched the strength requirements according to the related design code. The thermal performance of the tenon composite block wall was also good compared with that of a common block wall.

1. Introduction

Large amount of energy consumption and CO_2 emissions have caused serious environmental damage in recent years due to rapid urbanization. Climate change and energy conservation are seriously concerned. As a result, architectural concepts of "ecological cities," "green buildings," "building energy conservation," and "low-carbon buildings" have been gradually applied [1–3]. Statistical data indicate that heating, ventilation, and air-conditioning systems for buildings comprise approximately 50% of the building energy consumption and 20% of the total energy consumption in the United States [4, 5]. Table 1 shows the energy consumption percentage of different building parts, including the air-conditioning, illumination, kitchen, and water supply systems, and it can be seen that air-conditioning accounts for most of the energy consumption, which is related to the air temperature and the thermal performance of external maintenance components in a building. Some relevant statistical data also indicated that within the service age of buildings, the heat loss through external protection or structure components accounts for 70%–80% of the total heat loss [3], and the heat loss through external walls accounts for approximately 25% and 35% of the total heat loss during winter and summer, respectively [6, 7]. Thus, improving the thermal performance of building external walls is the key to reduce energy consumption in building service age.

In traditional masonry walls, fired clay brick has been widely used as a conventional masonry material for a long time. However, this led to excessive consumption of clay, energy, and resources and had a significant negative influence on the environment [8]. Thus, recently, new thermal insulation wall materials are playing key role in improving the thermal performance of external walls and realising green energy conservation in buildings. New concrete hollow blocks are effective replacements for traditional clay bricks. They have simplified construction and reduced construction time as the thermal materials have been integrated in the blocks, and additional external thermal construction is not needed [9–12].

However, in the development and application of new concrete hollow blocks, thermal performance and mechanical

Table 1: Energy consumption percentage of different building parts.

Energy category	Air condition	Illumination	Kitchen	Water supply
Proportion	65%	14%	6%	15%

performance are still limited. The polystyrene material has been proved as one of the most effective thermal insulation materials, of which the thermal conductivity is only 0.3 W/(m·K) and very close to that of air [13]. But the application of polystyrene, when used as polystyrene layer integrated in building walls, may cause unreliable connecting between thermal insulation layer with the main block or wall part and reduce the service age. The application of metal fasteners including steel bars was able to fix the polystyrene thermal insulation layer, but heat bridge caused by steel bars was very serious and reduced the total thermal performance [14–16]. So the thermal performance and mechanical performance are still limited and need to be balanced in application when using polystyrene material in new hollow blocks.

Based on the energy conservation requirements, a new tenon composite block (TCB) is proposed as the external maintenance component in building, as shown in Figure 1. The TCB consists of the internal hollow concrete block part and the external block part, which includes the concrete decoration layer at the block surface and the extruded polystyrene layer fixed by tenons between the internal hollow block part and decoration layer. The staggered arrangement of tenons in the TCB improves the connecting strength between the internal block and thermal insulation layer. Moreover, the staggered arrangement tenon prevents the reduction of the thermal insulation thickness and ensures the stability of the thermal insulation performance. This study focused on the strength and thermal performance of the TCB. By the optimization of concrete mixing ratio, the strength testing on single TCB, the thermal experimental test, and the finite element simulation of TCB specimens, the mechanical and thermal performance of TCB has been proved. Figure 2 shows the main contents and study procedure of this study.

2. Tenon Composite Block

2.1. Initial Concrete Mixing Ratio of Block Material. As the tenon composite block is produced by vibrating and pressing concrete materials into specially manufactured steel mold, the concrete material needs good molding performance. The initial concrete mixing ratio of TCB was determined based on the experience obtained from early preproduction of concrete block molding, manufacturing, and casting conditions in the laboratory. The initial concrete mixing ratio of the TCB was 20% gravel, 20% stone powder, 40% medium sand, 12% fly ash, 7% water-reducing agent, and 6% water.

2.2. Block Manufacturing Mold. The traditional block molding approach includes two steps: (1) the molding of the internal block part, which is used to bear loads and was completely made of concrete; (2) the connecting between the internal block part and the external heat insulation part. The

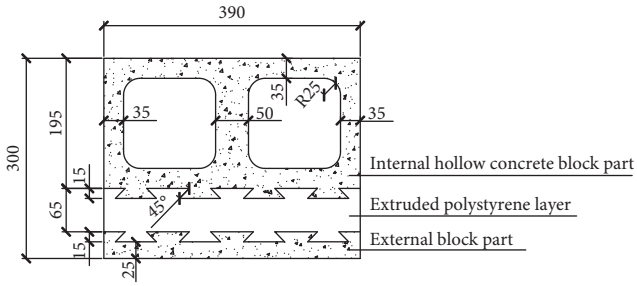

Figure 1: The tenon composite block (mm).

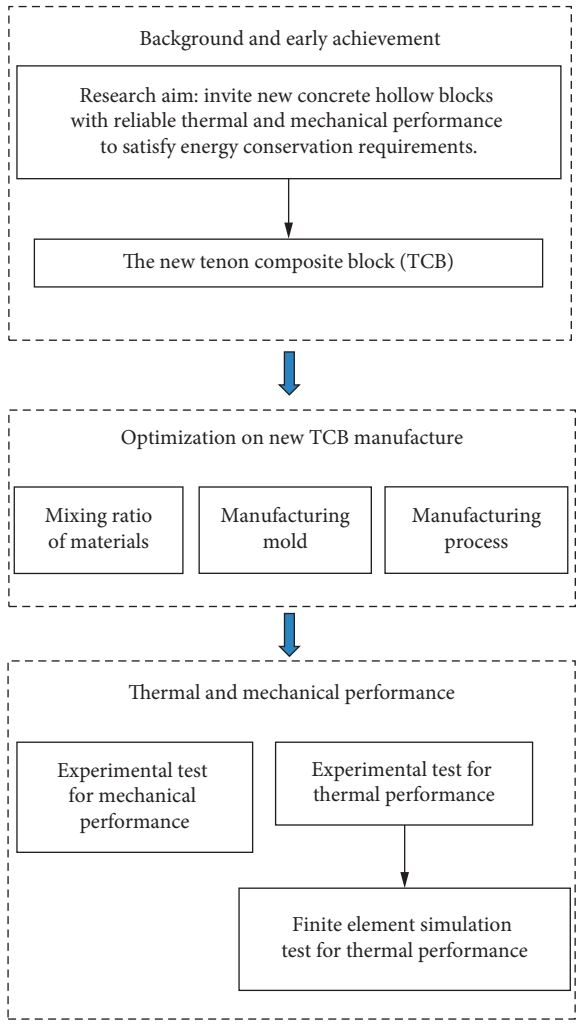

Figure 2: Main contents and study procedure of this study.

traditional molding approach is complicated due to the two separated steps and leads to unreliable connection performance between the internal block part and the external heat insulation part, which may cause service lifetime reduction due to temperature stresses between internal and external block parts. To avoid the service lifetime reduction caused by the traditional block molding approach, this study applied a new molding approach. The new one-step molding approach only contains one molding step according to the block shape, size, and experimental manufacturing condition. The mold for the new one-step block manufacturing is shown in Figure 3.

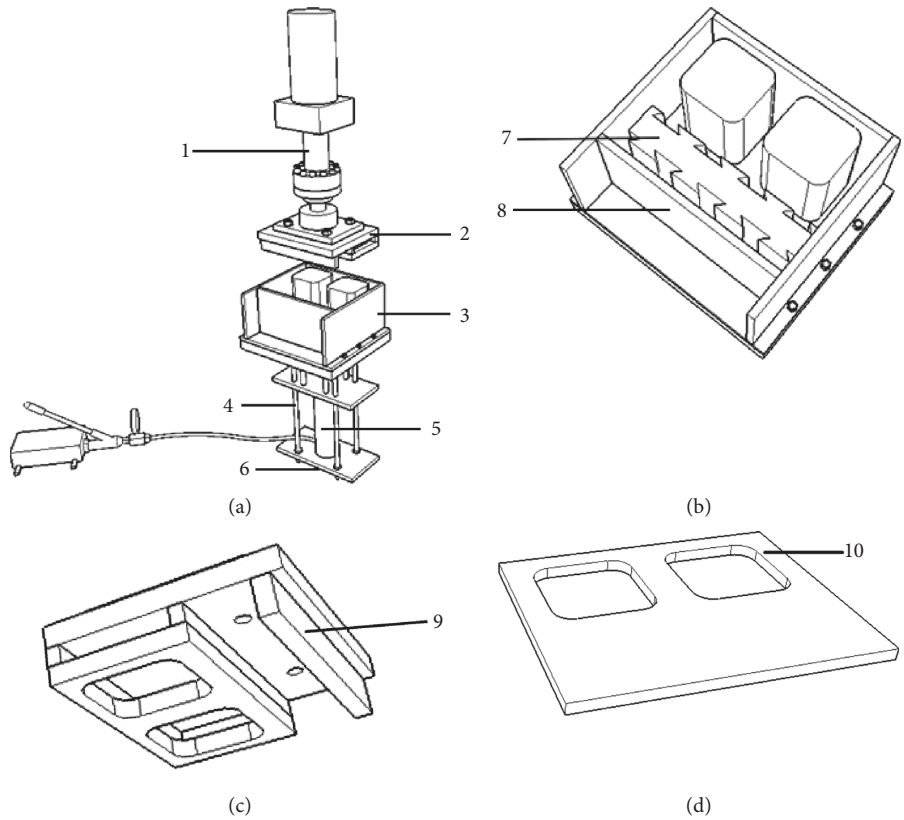

Figure 3: Block manufacturing equipment. (1) Upper hydraulic jack; (2) upper mold plate; (3) block mold; (4) supporting screw; (5) base hydraulic jack; (6) base fixing plate; (7) extruded polystyrene layer; (8) movable side plate of block mold; (9) upper mold plate; (10) block locating plate. (a) The whole block manufacturing system. (b) Details of the block mold. (c) Details of the upper block plate. (d) Details of the block support plate.

2.3. Optimized Mixing Ratio of TCB Concrete. In early concrete production for new TCB, one problem was found that the fine stone with 5 mm–16 mm diameter has an undesirable influence on concrete properties because it combines with water and cement to form large mud block and hinders the hydration reaction [9]. To avoid the damaging influence from fine stone with large diameter, mechanical basalt sand with a diameter of 2 mm–5 mm, which also has a lower thermal conductivity than traditional limestone, was applied as coarse aggregates to optimize the concrete properties and thermal performance.

By using the mechanical basalt sand, the mixing ratio of raw materials needs to be verified. To optimize the materials mixing ratio, the following measures were adopted:

(1) More water was needed because the mechanical stone is rough with more sharp edges and has low gradation properties, which may influence the concrete strength and mechanical properties. The stone powder was added into the concrete mixing ratio to fill the gaps between concrete aggregates and to improve the compactness and strength of concrete. To achieve better thermal performance, limestone powder was the final selection.

(2) Ceramsite is a lightweight aggregate produced by foaming in a rotary kiln and has spherical shape, smooth and hard surface, low density, low thermal conductivity, and high strength. It was added to the mixing ratio of raw materials to optimize the thermal and mechanical properties of concrete. Additionally, to avoid forming large blocks of mud, the diameter of the ceramsite particles was controlled to be lower than 5 mm.

(3) The content of fly ash was increased to improve the concrete strength, durability, thermal properties, and water absorption properties and to generate "bridges" and cavities inside the concrete material to reduce the thermal conductivity [17].

According to the above measures, two mixing ratios of A and B were designed, which differ from the mechanical sand and stone powder proportions. The A and B mixing ratios are shown in Table 2. The actual performance of the two mixing ratios was evaluated in the following mechanical and thermal tests.

2.4. Manufacturing Process. The manufacturing process procedure is shown in Figure 4. After the block manufacturing equipment was placed in correct position, the extruded polystyrene heat insulation layer can be placed into the block mold after lubricant was brushed on mold sidewalls, as shown in Figure 5.

The concrete production process contains two steps: the first step is a 20-second premixing step in a vertical material mixer to prepare uniform mixture of concrete raw materials

Table 2: Optimized A and B mixing ratios (%).

	Cement	Gravel (mechanical sand)	Stone powder	Ceramsite	Medium sand	Fly ash	Water-reducing agent	Water
Initial ratio	20	20	33		12	7	2	6
Mixing ratio A	18	25	18	8	10	10	2	9
Mixing ratio B	18	18	25	8	10	10	2	9

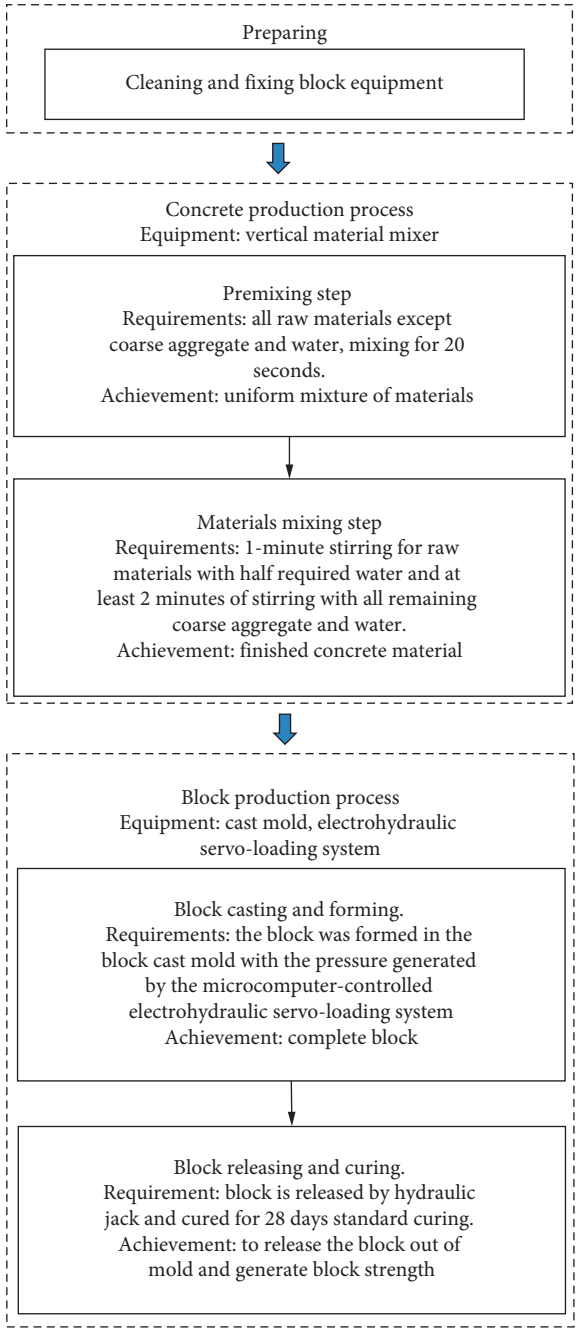

Figure 4: Manufacturing process of the new TCB.

which consists of cement, stone powder, fly ash, and water-reducing agent according to the mixing ratio; the coarse aggregate and water are not included in this step. The second step consists of stirring for 1 minute with 1/2 of the required water and at least 2 minutes of stirring after the addition of all the remaining coarse aggregate and water.

Figure 5: The extruded polystyrene heat insulation layer location in the mold.

After the prepared hard concrete was added into the block cast mold, the block was formed with the pressure generated by the microcomputer-controlled electrohydraulic servo-loading system, as shown in Figure 6. Following the block formation, the block can be easily released by lifting the upper hydraulic jack, as shown in Figure 7.

The block products are shown in Figure 8. The curing process for all blocks was in the natural environment, where the blocks were covered with straw and watered for the first 14 days after the blocks were released. A TCB after 28 days of standard curing is shown in Figure 9.

3. Strength Test

Ten blocks from each mixing ratio (A and B) were randomly selected and divided into two groups to test the strength. Each group contained five blocks from every mixing ratio. One group (5 from A and 5 from B) was tested after block production. The blocks in the other group (5 from A and 5 from B) were tested after being placed for 6 months in open-air conditions. The strength tests used a WAW-1000 electrohydraulic servo-testing machine. The loading speed was controlled to be 0.2–0.3 MPa/s, and the loading continued until a vertical crack appeared on the block according to "Test Methods for the Concrete Block and Brick" [18]. Limited by experimental conditions of the WAW-1000 electrohydraulic servo-testing machine, the effect of porosity and eccentricity were not considered in the strength test. The average compressive strengths are shown in Table 3.

The average compressive strength for each case is shown in Table 3. Effect of porosity and eccentricity on the mechanical properties can be found. The strength requirement of 5 MPa [19] was exceeded for each case, meaning that the three concrete mixing ratios can be applied to blocks used as infill walls and load-bearing walls in multilayer masonry structures. As in the block manufacturing process, the porosity was mainly controlled in the materials stirring and

(a) (b)

Figure 6: Blocks being formed. (a) Concrete being prepared. (b) Pressure being applied by a hydraulic jack.

Figure 7: Upper hydraulic jack being lifted to release the block.

Figure 9: Block after the curing process.

Figure 8: Blocks being cured.

block casting step in the manufacturing process, the testing strength of TCB matched the strength requirements of design codes, proving that the porosity was well controlled in the manufacturing process.

The compressive strength of mixing ratio A is less than 5% that of mixing ratio B. The main difference between mixing ratio A and B is the portion of mechanical sand and stone powder. The mechanical sand percentage in mixing ratio A is higher, but as a coarse aggregate, mechanical sand improved the strength and reduced the thermal insulation performance. Therefore, the thermal insulation performance of mixing ratios A and B is discussed below in Section 3 together with mechanical performance.

Blocks with the A and B mixing ratios with open-air placing for 6 months after manufacture have 7.7% and 4.1% higher in average compressive strengths, respectively, than the A and B mixing ratio blocks after production. This means the chemical reaction of material components continued to increase the strength with time. Finally, the TCB with the initial concrete mixing ratio had the highest strength of 8.15 MPa compared to that of ratios A and B, meaning that the optimization of the thermal performance caused a reduction in the block compressive strength.

4. Thermal Testing

4.1. Thermal Testing Apparatus and Specimens. The WTRZ-1212 steady-state heat transfer performance testing machine was used for this test, which was developed and produced strictly according to the requirements in the national test standard of "Building Element-Determination of Steady-State

Table 3: Average compressive strength of blocks (MPa).

Mixing ratio	A	B	A (6 months in open air)	B (6 months in open air)	Initial mixing ratio
Compressive strength	6.88	6.57	7.41	6.84	8.15

Thermal Transmission Properties—Calibrated and Guarded Hot Box" (GB/T13475-2008) in China [17]. The maximum sample size for standard WTRZ-1212 is 1.64 m × 1.64 m, and the measuring size of the TCB wall specimen is 1.2 m × 1.2 m. The testing machine is shown in Figure 10. The test is based on the guarding hot-box method, which relies on a heat protective box to balance external and internal environments and quantitatively analyze thermal performance with minimized heat consumption and high accuracy. The box is also optimized to reduce error by synthetically measuring the heat loss of test instruments. The testing machine and specimen in reality are shown in Figure 11.

Three TCB wall specimens were tested to compare the thermal performance using different concrete mix proportions: initial mixing ratio and the A and B mixing ratios. The block and wall parameters are shown in Table 4. Table 5 shows the initial parameters used for the thermal test.

4.2. Thermal Test Results. The three TCB wall specimens were tested strictly according to the national test standard of "Building Element-Determination of Steady-State Thermal Transmission Properties—Calibrated and Guarded Hot Box" (GB/T13475-2008) [17]. In the test, the heating power Q_p of the heating machine shown in Figure 12 will be collected. Apart from that, the temperature difference θ_3 between the inner wall and the outer wall of shelter in heating part (Figure 12), the hot surface temperature T_{si} and the cool surface temperature T_{se} of the specimen, the air temperature of protective hot box T_{ni} and the air temperatures of cool box T_{ne} will be collected, among which the T_{ni} and T_{ne} were set to be 30°C and −10°C in the test but were still collected to consider testing errors and to improve testing accuracy. The thermal parameters of the three block wall specimens can be calculated from the collected data and according to equations (1)—(5), shown in Table 6, including the thermal resistance, the thermal conductivity, the heat transfer coefficient, and the total thermal resistance:

$$Q_1 = Q_p - M_3\theta_3, \tag{1}$$

$$R = \frac{A(T_{si} - T_{se})}{Q_1}, \tag{2}$$

$$\lambda_k = \frac{\delta}{R}, \tag{3}$$

$$K = \frac{Q_1}{[A(T_{ni} - T_{ne})]}, \tag{4}$$

$$R_{su} = \frac{1}{K}. \tag{5}$$

From the thermal parameters in Table 6, the following conclusions can be drawn:

(1) The TCB specimens have good total thermal performance when compared the total thermal resistance R_{su} to the R_{su} value of 3.0 m^2 · K/W of common block wall, in which the block has three rows of heat isolation holes and size of 390 mm × 190 mm × 190 mm. The R_{su} values of the TCB wall are 6.10, 6.50, and 6.70 times of the total thermal resistance of common block wall for the Q-1, the Q-2, and the Q-3, respectively.

(2) According to the total thermal resistance R_{su} values of the three wall specimens of Q-1, Q-2, and Q-3, the heat insulation properties of the TCB walls with mixing ratios A and B are 6.56% and 9.84% higher than that of specimen with the initial mixing ratio, respectively, which indicates that the mixing ratio and production processing optimization have improved thermal performance. As this study concluded in Section 2 that the TCB with the initial concrete mixing ratio had the highest strength of 8.15 MPa compared to that of ratios A and B, together with the R_{su} values differences between Q-1 to Q-2 and Q-3, it can be proved that by the optimization of concrete mixing ratio, the thermal performance was improved and the block compressive strength was reduced. Based on the above conclusions, it is suggested that the two optimized mixing ratios and block production process should be used in TCB production.

(3) The total thermal resistance R_{su} of the block wall with the mixing ratio A (Q-2) is 3.08% lower than that of the block wall with mixing ration B (Q-3), meaning that the heat isolation properties of the mixing ratio A wall are better than that of the mixing ratio B wall. According to the block compressive strength shown in Table 3 and the results in Section 2, the compressive strength of mixing ratio A is less than 5% that of mixing ratio B. Together with thermal parameters in Table 6, it can be insufficiently proved that the portion of mechanical sand and stone powder is the key to control thermal insulation and mechanical performance: more mechanical sand can improve the strength and more stone powder can improve the thermal insulation performance. But when considering there is a difference of 3.08% in R_{su} between the A and B mixing ratios, however, the trend is not obvious when considering the 7% difference in the mechanical sand and stone powder percentages in the A and B mixing ratios. The influence of mechanical sand and limestone powder

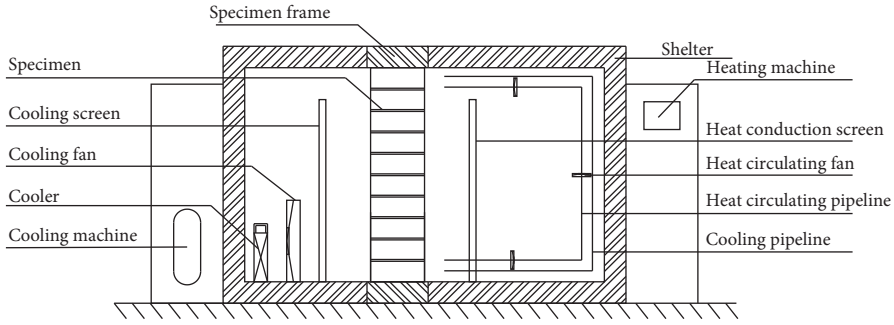

Figure 10: Schematic of the test machine for the joggled joint block wall thermal test.

Figure 11: Testing machine in reality.

Table 4: Specimen parameters.

Specimen	Block	Size (mm)
Q-1	Initial mixing ratio block	390 × 300 × 115
Q-2	A mixing ratio block	390 × 300 × 115
Q-3	B mixing ratio block	390 × 300 × 115

Table 5: Initial parameters used for the thermal test.

Air temperature of experimental heat box	30.0°C
Air temperature of protective hot box	30.0°C
Air temperature of cold box	−10.0°C
Relative humidity of experimental heat box	30%
Heat flux coefficient M_3 of the external wall of measuring heat box	1.52 W/K
Wall thickness	300 mm

percentage should be further evaluated based on more test cases.

5. Finite Element Simulation

5.1. Finite Element Model. The thermal analysis module integrated in ANSYS finite element simulation software was used to simulate the thermal performance of the TCB wall in heated steady state. In the thermal simulation of wall specimen in this study, as the wall size is 1.2 m × 1.2 m × 0.2 m, of which the specimen front face sizes are much larger than the specimen thickness, the heat energy flow simulation will be simplified to be one-dimensional heat conduction simulation on the two-dimensional finite element model, which only considers the heat energy flow in the thickness direction. And as the thermal experimental testing was the steady-state heat transfer performance testing, the finite element simulation will also assume that the specimen was in steady-state heat transfer situation. Finally, the finite element simulation adopted the following three assumptions:

(1) Different material parts in TCB, including the internal hollow concrete block part, the extruded polystyrene layer, and the external block part, will be assumed to be inseparable connected and no material or thermal properties changes with temperature.

(2) The heat energy flow will only be in the thickness direction, and the simulation will be simplified to be one-dimensional heat conduction simulation.

(3) The simulation of the specimen is in the steady-state heat transfer situation, which means the environment temperature of the two sides of the specimen remains constant.

Based on the above assumptions and test method [20–22], the simulation element for the TCB wall was selected as PLANE55, which is a two-dimensional thermal solid element with 4 nodes and can be used as a planar or axisymmetric element in two-dimensional heat steady-stage and instantaneous-stage analyses [23]. The node in the PLANE55 element only contains one temperature degree of freedom.

5.2. Material Properties. According to the experimental test results and the theory of the parallel-series method in equations (1)—(5), the thermal conductivity of the concrete for mixing ratio A can be calculated as $\lambda_k = 1.178\text{W}/(\text{m}\cdot\text{K})$. Other thermophysical parameters of related materials used in the TCB are determined according to the testing standard of "Code for Thermal Design of Civil Building" (GB 50176-2016) [24] and are shown in Table 7.

5.3. Meshing and Boundary Conditions. The finite element geometric model was automatically generated by the ANSYS

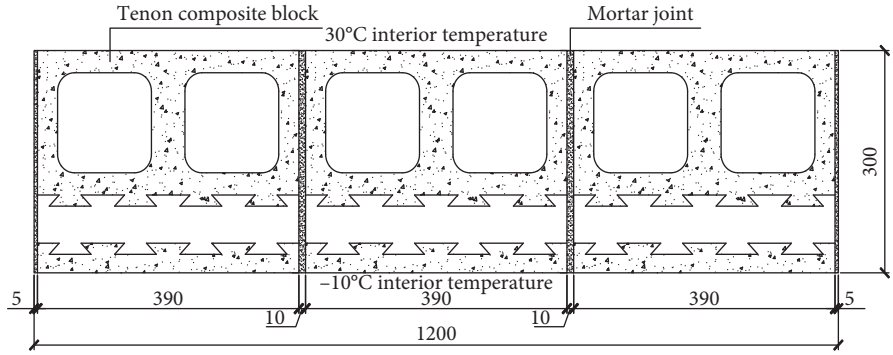

Figure 12: Simplified heat transfer model of the block wall.

Table 6: Thermal parameters of test specimens.

Specimen	Thermal resistance R (m^2·K/W)	Thermal conductivity λ_k (W/(m·K))	Heat transfer coefficient K (W/(m^2·K))	Total thermal resistance R_{su} (m^2·K/W)
Q-1	1.581	0.632	0.546	1.830
Q-2	1.691	0.591	0.513	1.950
Q-3	1.765	0.567	0.497	2.010

Table 7: Thermophysical parameters of materials in TCB.

Material	Thermal conductivity (W/(m·K))	Thickness (mm)
Concrete	1.178	195
Extruded polystyrene layer	0.030	65
Vertical air interlayer	0.746	135
Masonry mortar	0.930	25

simulation software, and the mesh was discretized into a triangle or quadrilateral shape with 5 mm mesh size. Compared with the thermal experimental test results of the wall, the interior temperature of the simulated wall was 30°C, and the exterior temperature of the wall was −10°C. The finite element simulation model assumed that the boundary conditions are complete heat isolation: the convective heat transfer is only applied on internal and external surfaces which are selected as boundary condition, while no heat transfer exists on block connection joints. The convective heat transfer coefficients of the interior and exterior were 8.7 W/(m^2·K) and 23.0 W/(m^2·K), respectively. The simplified one-dimensional TCB wall model is shown in Figure 12. The ANSYS geometric model is shown in Figure 13. The mesh used for the joggled joint block wall model is shown in Figure 14.

5.4. Simulation Results. The finite element simulation calculated the temperature distribution and heat flux distribution maps shown in Figures 15 and 16. According to the heat flux distribution map, the average heat flux density Q_1 can be obtained by ANSYS software. And according to Fourier's law of heat conduction in equation (2), the thermal conductivity value can be obtained. The relation between specimen total thermal resistance and thermal conductivity can be obtained by equation (3). The average thermal performance parameters of the wall specimen are shown in Table 8. By comparing the calculation results with those obtained in the previous experimental test, it can be found that the numerical simulation thermal resistance of the A mixing ratio block wall is 2.133 (m^2·K)/W, which is 6.1% higher than that obtained from experimental testing of 1.950 (m^2·K)/W. The relative error is caused by two reasons: (1) the simulation model assumes that the boundary conditions are complete heat isolation and inconsistent with reality; (2) heat loss and measurement error are inevitable in the experimental test process. Comparing the simulation results with the experimental results, the relative error is low and acceptable.

Figure 15 shows the temperature distribution of the TCB wall, where it can be seen that the temperature decreases gradually from the internal surface to the external surface. However, the area with the most rapid temperature decrease was the heat isolation layer. Because temperature variation rate is inversely proportional to the thermal conductivity value of the material, and the thermal conductivity value of the extruded polystyrene layer is 0.030W/(m·K), which is far less than the value of 1.178W/(m·K) for concrete and 0.746W/(m·K) for air, it can be proved that the extruded polystyrene layer contributes most of the heat isolation performance. It can be found in Figure 15 that the temperature boundary lines of 21°C and 25°C exhibited obvious fluctuations: there was a high temperature distribution area in the middle position of block, while low temperature distribution area is close to the block joint, proving the existence of thermal bridge caused by the block joints. However, because the main heat isolation component is the extruded polystyrene layer, the fluctuate depth of temperature was limited in the concrete part and no temperature influence reached at the external surface.

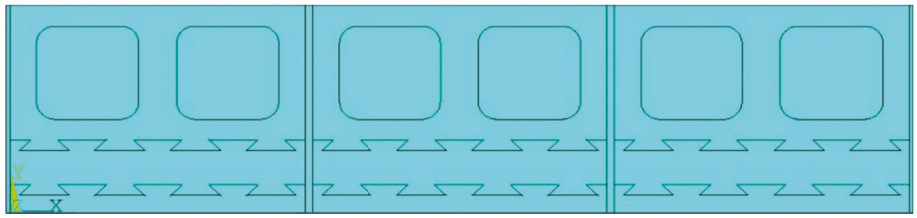

Figure 13: Geometric model of the thermal analysis unit.

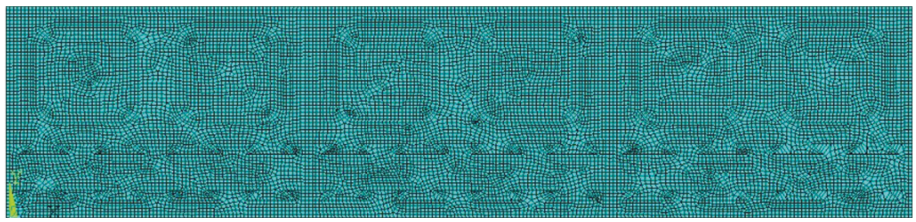

Figure 14: Grid diagram of the thermal analysis unit.

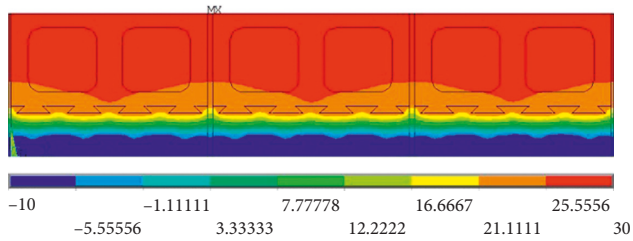

Figure 15: Cloud pattern of wall temperature distribution.

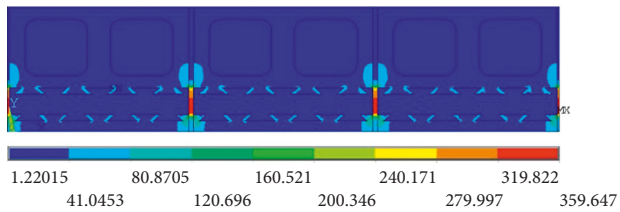

Figure 16: Distribution of heat flux density in the wall.

Table 8: Total thermal resistance of the block wall in the experimental test and numerical simulation.

Condition	Total thermal resistance R_u ($m^2 \cdot K$)/W	Relevant error
Experiment	2.010	6.1%
Numerical simulation	2.133	

Figure 16 is the heat flux density distribution of the tenon connected block wall model in heat steady stage. The heat flux density in most of the wall area is very low, including the internal hollow concrete part, the extruded polystyrene layer, and the external concrete part, which indicated that the extruded polystyrene layer and the air insulation layer effectively prevent heat transmission. However, a very high heat flux density distributed at the block joints, which proved the same phenomenon of the thermal bridge in Figure 15.

Concluding the temperature and heat flux density distribution in Figures 15 and 16, the extruded polystyrene layer contributed very reliable and continuous thermal insulation performance, which contributed to the staggered arranged tenon avoiding the thickness reduction of extruded polystyrene layer. This also proved the reasonability of the staggered arranged tenon in this new TCB. Apart from the reasonably arranged tenon, the block joint still inevitably becomes the heat bridge of tenon composite thermal insulation wall and further study on avoiding heat bridge of block joint should be focused.

6. Conclusion

The main conclusions obtained from the experimental testing and numerical simulation are as follows:

(1) The experimental strength test of the blocks with three different mixing ratios, which were proposed by early experimental test experiences and optimization, proved that the mixing ratios were reliable to supply higher strength than the design code required strength.

(2) The experimental steady-state thermal test on TCB wall specimens indicated that the TCB wall specimen has good thermal performance when compared to the total thermal resistance with the common block wall.

(3) Experimental results from the thermal test and the mechanical test proved that the A mixing ratio block had better thermal performance, which contributes to the mechanical sand and stone powder percentages, while very close strength to that of B mixing ratio block. Therefore, it is suggested that the optimized A mixing ratio can be used in the TCB production.

(4) The numerical simulation provided acceptable and accurate results with a low relative error. The numerical simulation results proved the reasonability of the staggered arranged tenon to avoid thermal performance reduction. But the inevitable thermal bridge existed at the block joints and should be focused in further study.

Nomenclature

Basic Units

K: Kelvin temperature
MPa: Mega Pascal
m: Meter
mm: Millimeter
W: Watt
s: Second
°C: Celsius temperature

Latin and Greek letters

A: Face area of specimen (m^2)
K: Heat transfer coefficient ($W/(m^2 \cdot K)$)
M_3: Heat flux coefficient of external wall of measuring heat box (W/K)
Q_1: Heat flux rate (W)
R: Thermal resistance ($m^2 \cdot K/W$)
R_{su}: Total thermal resistance ($m^2 \cdot K/W$)
δ: Specimen thickness (m)
λ_k: Thermal conductivity ($W/(m \cdot K)$)

Acronyms

CO_2: Carbon dioxide
TCB: Tenon composite block.

Data Availability

The data used to support the findings of this study are available from the corresponding author upon request.

Conflicts of Interest

The authors declare that they have no conflicts of interest.

Acknowledgments

This work was supported by the Science Project of Jiangsu Water Conservancy Bureau (Grant no. 2016038), the Social Development Project of Nanjing Science and Technology Commission Fund Programs (Grant no. 201505018), and the National Natural Science Foundation for Young Scientists of China (Grant no. 51708260).

References

[1] A. N. Raut and C. P. Gomez, "Assessment of thermal and energy performance of thermally efficient sustainable wall system for Malaysian low cost housing," *Applied Thermal Engineering*, vol. 136, pp. 309–318, 2018.

[2] G. Vasconcelos, P. Lourenco, P. Mendonca et al., "Proposal of an innovative solution for partition walls: mechanical, thermal and acoustic validation," *Construction and Building Materials*, vol. 48, pp. 961–979, 2013.

[3] R. D. Diao, L. Z. Sun, and F. Yang, "Thermal performance of building wall materials in villages and towns in hot summer and cold winter zone in China," *Applied Thermal Engineering*, vol. 128, pp. 517–530, 2018.

[4] V. Echarri-Iribarren, C. Rizo-Maestre, and F. Echarri-Iribarren, "Healthy climate and energy savings: using thermal ceramic panels and solar thermal panels in mediterranean housing blocks," *Energies*, vol. 11, no. 10, 2018.

[5] M. Fogiatto, G. Santos, and J. Catelan, "Numerical two-dimensional steady-state evaluation of the thermal transmittance reduction in hollow blocks," *Energies*, vol. 12, no. 3, p. 449, 2019.

[6] E. Wati, P. Meukam, and J. C. Damfeu, "Modeling thermal performance of exterior walls retrofitted from insulation and modified laterite based bricks materials," *Heat and Mass Transfer*, vol. 53, no. 12, pp. 3487–3499, 2017.

[7] A. Laaouatni, N. Martaj, R. Bennacer, M. Lachi, M. El Omari, and M. El Ganaoui, "Thermal building control using active ventilated block integrating phase change material," *Energy and Buildings*, vol. 187, pp. 50–63, 2019.

[8] J. Wu, G. L. Bai, P. Wang, and Y. Liu, "Mechanical properties of a new type of block made from shale and coal gangue," *Construction and Building Materials*, vol. 190, pp. 796–804, 2018.

[9] M. X. Xiong, Y. H. Wang, and J. Y. R. Liew, "Evaluation on thermal behaviour of concrete-filled steel tubular columns based on modified finite difference method," *Advances in Structural Engineering*, vol. 19, no. 5, pp. 746–761, 2016.

[10] D. Y. Wu, S. T. Liang, M. Y. Shen, Z. X. Guo, X. J. Zhu, and C. F. Sun, "Experimental estimation of seismic properties of new precast shear wall spatial structure model," *Engineering Structures*, vol. 183, pp. 319–339, 2019.

[11] D. Y. Wu, S. T. Liang, M. Y. Shen et al., "Finite-element simulation on NPGCS precast shear wall spatial structure model," *Advances in Civil Engineering*, vol. 2019, Article ID 2647891, 17 pages, 2019.

[12] S. Noor-E-Khuda and F. Albermani, "Mechanical properties of clay masonry units: destructive and ultrasonic testing," *Construction and Building Materials*, vol. 219, pp. 111–120, 2019.

[13] I. Gnip, S. Vejelis, and S. Vaitkus, "Thermal conductivity of expanded polystyrene (EPS) at 10 degrees C and its conversion to temperatures within interval from 0 to 50 degrees C," *Energy and Buildings*, vol. 52, pp. 107–111, 2012.

[14] T. Theodosiou, K. Tsikaloudaki, S. Tsoka, and P. Chastas, "Thermal bridging problems on advanced cladding systems and smart building facades," *Journal of Cleaner Production*, vol. 214, pp. 62–69, 2019.

[15] P. Brzyski, M. Grudzinska, and D. Majerek, "Analysis of the occurrence of thermal bridges in several variants of connections of the wall and the ground floor in construction Technology with the use of a hemp-lime composite," *Materials*, vol. 12, no. 15, 2019.

[16] M. Khoukhi, "The combined effect of heat and moisture transfer dependent thermal conductivity of polystyrene insulation material: impact on building energy performance," *Energy and Buildings*, vol. 169, pp. 228–235, 2018.

[17] GB/T13475-2008, *Building Element-Determination of Steady-State Thermal Transmission Properties–Calibrated and Guarded Hot Box*, China Architecture & Building Press, Beijing, China, 2008.

[18] GB/T4111-2013, *Test Methods for the Concrete Block and Brick*, China Architecture & Building Press, Beijing, China, 2013.

[19] GB50003-2011, *Code for Design of Masonry Structures*, China Architecture & Building Press, Beijing, China, 2011.

[20] H. Yang, X. Xu, W. Xu, and I. Neumann, "Terrestrial laser scanning-based deformation analysis for arch and beam structures," *IEEE Sensors Journal*, vol. 17, no. 14, pp. 4605–4611, 2017.

[21] H. Yang, X. Xu, and I. Neumann, "Deformation behavior analysis of composite structures under monotonic loads based on terrestrial laser scanning Technology," *Composite Structures*, vol. 183, pp. 594–599, 2017.

[22] H. Yang, X. Xu, and I. Neumann, "Laser scanning-based updating of a finite-element model for structural health monitoring," *IEEE Sensors Journal*, vol. 16, no. 7, pp. 2100–2104, 2016.

[23] V. Koci, J. Koci, J. Madera et al., "Thermal and hygric assessment of an inside-insulated brick wall: 2D critical experiment and computational analysis," *Journal of Building Physics*, vol. 41, no. 6, pp. 497–520, 2018.

[24] GB 50176-2016, *Code for Thermal Design of Civil Building*, China Architecture & Building Press, Beijing, China, 2016.